

Deriving Health Metrics from the Photoplethysmogram: Benchmarks and Insights from *MIMIC-III-Ext-PPG*

Mohammad Moulaeifard*, Philip J. Aston^{†‡}, Peter H. Charlton[§], Nils Strodthoff**

*AI4Health Department, Oldenburg University, Oldenburg, Germany

[†]Department of Data Science and AI, National Physical Laboratory, Teddington, United Kingdom

[‡]School of Mathematics and Physics, University of Surrey, Guildford, United Kingdom

[§]Department of Public Health and Primary Care, University of Cambridge, Cambridge, United Kingdom

*Corresponding author: nils.strodthoff@uol.de

Abstract—Photoplethysmography (PPG) is one of the most widely captured biosignals for clinical prediction tasks, yet PPG-based algorithms are typically trained on small-scale datasets of uncertain quality, which hinders meaningful algorithm comparisons. We present a comprehensive benchmark for PPG-based clinical prediction using the *MIMIC-III-Ext-PPG* dataset, establishing baselines across the full spectrum of clinically relevant applications: multi-class heart rhythm classification, and regression of physiological parameters including respiratory rate (RR), heart rate (HR), and blood pressure (BP). Most notably, we provide the first comprehensive assessment of PPG for general arrhythmia detection beyond atrial fibrillation (AF) and atrial flutter (AFLT), with performance stratified by BP, HR, and demographic subgroups. Using established deep learning architectures, we achieved strong performance for AF detection (AUROC = 0.96) and accurate physiological parameter estimation (RR MAE: 2.97 bpm; HR MAE: 1.13 bpm; SBP/DBP MAE: 16.13/8.70 mmHg). Cross-dataset validation demonstrates excellent generalizability for AF detection (AUROC = 0.97), while clinical subgroup analysis reveals marked performance differences across subgroups by BP, HR, and demographic strata. These variations appear to reflect population-specific waveform differences rather than systematic bias in model behavior. This framework establishes the first integrated benchmark for multi-task PPG-based clinical prediction, demonstrating that PPG signals can effectively support multiple simultaneous

monitoring tasks and providing essential baselines for future algorithm development.

Index Terms—Decision support systems, Photoplethysmography, Machine learning, algorithms, Signal processing, Time series analysis

I. INTRODUCTION

Photoplethysmography (PPG) has become one of the most widely available biosignal monitoring technologies in contemporary healthcare, delivering non-invasive, continuous physiological monitoring functionality in a wide range of clinical contexts [1], [2]. PPG sensors are used from the intensive care unit (ICU) to consumer wearables, offering real-time physiological information about cardiovascular and respiratory function through the optical measurement of the blood volume variations in peripheral tissues [3], [4].

PPG-based prediction tasks Recent machine learning advances have shown the promise of PPG for arrhythmia detection [5]–[7], BP estimation [8]–[10], and RR estimation [11], [12], to name just a few prominent applications.

Limitations of existing benchmarking studies Although several benchmark studies have attempted

to evaluate PPG-based prediction tasks, these efforts are hindered by certain methodological limitations. The benchmarking studies for RR estimation, e.g., [13], [14], HR estimation, e.g., [15], and BP prediction, e.g., [16], provide useful and informative insights. However, these studies mostly evaluate isolated prediction tasks and rely on relatively constrained datasets, which limits their ability to generalize across populations and physiological conditions. Also, they rarely incorporate multi-task learning or leverage rich clinical metadata, leaving important aspects of real-world physiological monitoring unexplored.

Finegrained rhythm classification from PPG In terms of arrhythmia classification, existing PPG-based studies have focused on addressing limited and narrowly defined scenarios, such as AF vs. non-AF, abnormal rhythm detection beyond AF, or multiclass settings with a relatively low number of rhythm classes [5], [17]–[19]. As a result, the fine distinction between rhythms across a large number of clinically relevant classes remains largely unexplored. Moreover, the evaluation of model performance on clinically relevant classes, such as those based on BP, HR, or demographic features, is not commonly performed. All these issues underscore the need for a comprehensive and multi-task benchmarking approach to PPG analysis, as presented in this work.

Dataset considered in this work The recent large-scale, quality-assessed PPG dataset *MIMIC-III-Ext-PPG* [20] addresses these limitations by offering several key advantages over existing datasets. It provides the most comprehensive task coverage, includes over 6.3 million 30-second PPG segments from 6,189 intensive care patients, supporting both extensive heart rhythm classification (26 classes) and physiological parameter regression (BP, HR, RR). The dataset includes rich clinical metadata encompassing demographics, ethnicity, biometrics, and comorbidities, enabling thorough subgroup analysis.

Contributions In this work, we introduce a comprehensive benchmarking framework consolidating both classification and regression tasks for PPG-based clinical prediction. Our rigorous assessment

includes heart rhythm classification at multiple granularities, physiological parameter regression, such as RR, HR, and BP estimation. We set up performance baselines using well-known deep learning architectures and investigate model generalizability through out-of-distribution testing and clinical subgroup analysis. More specifically, the contributions of this study are the following: (1) we presented a benchmarking protocol for comprehensive PPG clinical prediction, demonstrating the feasibility of multi-task physiological monitoring from PPG signals; (2) we provided essential performance benchmarks for all major PPG clinical applications, facilitating standardized assessment for prospective algorithmic advancements; (3) in particular, we demonstrated the feasibility of finegrained arrhythmia classification based on PPG data alone; and (4) we revealed task-specific performance discrepancies among clinical and demographic subgroups (e.g., varying hypertension levels, HR categories, BMI, gender, and ethnicity in heart rhythm classification), offering critical insights for real-world deployment.

II. MATERIALS AND METHODS

A. Dataset and Task Definitions

Dataset summary We used the *MIMIC-III-Ext-PPG* dataset [20], [21], a comprehensive PPG-based benchmark (Table I). This dataset is derived from the MIMIC-III Waveform Database Matched Subset [22], containing recordings from critically-ill patients. It comprises 6,399,754 30-second PPG segments from 6,189 subjects, all annotated for heart rhythm classification. In addition, subsets provide labels for RR (4,695 subjects, 5,546,169 segments), HR (5,924 subjects, 5,187,183 segments), and BP (2,391 subjects, 2,468,693 segments).

Heart rhythm classification tasks We trained and evaluated models across two primary categories (regression and classification tasks) encompassing the full spectrum of clinically relevant PPG applications. Table IV presents each heart rhythm, the associated number of unique patients, the number of 30-second samples, and the corresponding rhythm abbreviation used in this paper. For heart rhythm classification, we distinguished three scenarios (tasks):

TABLE I: Demographic and clinical characteristics of the study population across different physiological subsets. Values are presented as mean \pm SD or percentage (%).

Metric	Heart rhythm	RR	HR	BP
Number of subjects	6,189	4,695	5,924	2,391
Number of segments (30s)	6,399,754	5,546,169	5,187,183	2,468,693
Total Duration (h)	\sim 53,331	\sim 46,218	\sim 43,227	\sim 20,572
Age (years, mean \pm SD)	64.1 \pm 17.0	65.0 \pm 16.1	63.9 \pm 16.9	63.2 \pm 16.2
Weight (kg, mean \pm SD)	82.2 \pm 22.6	82.0 \pm 21.8	82.3 \pm 22.6	83.2 \pm 21.9
Height (cm, mean \pm SD)	169.5 \pm 10.5	169.7 \pm 10.5	169.4 \pm 10.5	169.7 \pm 10.4
Gender (female, %)	43.9	43.3	44.0	42.2
Ethnicity (%)				
- White	72.0	73.5	72.0	71.4
- Black	9.2	9.3	9.1	7.7
- Hispanic	4.1	3.8	4.1	3.8
- Asian	2.8	2.8	2.9	3.0
- Other	11.9	10.6	11.9	14.1

- *Robust AF/AFLT detection (AF task)*: A multi-label classification task with two binary output nodes—one for AF detection and one for AFLT detection. This task setup aligns with typical AF/AFLT detection settings considered in the literature.
- *Sinus versus atrial arrhythmia discrimination (SAA task)*: A multi-label binary classification task with two binary output nodes – one to detect sinus rhythm (SINUS) and one to detect atrial arrhythmias (AF+AFLT). SINUS comprises SR, STACH, SBRAD, and SARRH, while AF+AFLT includes AF and AFLT. This task assesses the model’s ability to detect atrial rhythm disturbances while remaining robust to physiological variations within sinus rhythm.
- *Comprehensive rhythm classification (ARRH task)*: A multi-label classification task with 13 binary output nodes, each corresponding to a specific rhythm type. We included all 13 rhythm classes with more than 1,000 30-second samples, while all other well-defined rhythm types are included in OTHER. This task evaluates the possibility of fine-grained rhythm classification based solely on PPG signals.

It is worth noting that in all scenarios, we excluded all atrioventricular blocks as well as left and

right bundle branch blocks (LBBB and RBBB), as they can co-occur with different rhythm types. For all three tasks, we include all samples from the respective heterogeneous OTHER rhythm sample group with zero labels for all outputs to improve robustness to non-target rhythms. The complete mapping table is given Table IV.

Regression tasks For regression tasks, we evaluated continuous prediction of RR and HR (breaths/beats per minute), and simultaneous SBP/DBP estimation (mmHg) from the PPG. All labels are provided as columns in the *MIMIC-III-Ext-PPG* dataset.

B. Model Architectures and Experimental Setup

Model We used two established deep learning architectures: XResNet1d101 [23], a state-of-the-art ResNet architecture, and LeNet1D [24], a shallow convolutional model adapted to 1D time series as a baseline. Both models showed robust performance in a recent benchmarking study [16]. The XResNet1d101 model was chosen as a representative for a comparably deep, parameter-heavy model, and LeNet1D as a representative for a lightweight model.

Experimental setup *MIMIC-III-Ext-PPG* provided raw PPG segments without flatlines or NaN values. Further pre-processing of the signals was performed by utilizing the `ppg_clean` function provided by

the NeuroKit2 library [25]. The Elgendi algorithm was utilized, which includes a Butterworth bandpass filter between 0.5 and 8 Hz to reduce the baseline drift and high-frequency noise. The sampling rate was set at 125 Hz, and the models were trained at full input resolution of each segment, which was equivalent to 3750 time steps (30 seconds).

We leveraged the provided 10 folds, stratified according to heart rhythm events, age distributions, and cardiovascular diagnoses. The first seven folds were used for training, the eighth fold for validation, and the ninth and tenth folds for testing. For each experiment, an effective batch size of 512 was used through gradient accumulation. The learning rates were set to 0.001 for all models, and models were trained for 50 epochs. The training was implemented using the AdamW optimizer [26]. As a simple measure to reduce overfitting, we performed model selection based on the validation set score, i.e., during training, we kept track of the validation set score and selected the model with the best validation set score for evaluation on the test set. We used the macro averaged area under the receiver operating curve (AUROC) as a threshold-independent metric to characterize the overall discriminative power of the model for classification tasks and the mean absolute error (MAE) as the main metric for regression tasks.

BP estimation For BP estimation, consistent with previous studies, e.g., [27], [28], we employed two output nodes to jointly predict SBP and DBP, leveraging possibly shared physiological features to enhance model performance for both SBP and DBP.

Arrhythmia classification In all arrhythmia detection cases, we handled the heterogeneous set of remaining rhythm types by using a one-hot encoding and applying binary cross-entropy across all output channels. Although each sample belongs to exactly one rhythm class, this formulation treats the problem as a multi-class prediction with independent sigmoid outputs rather than a softmax layer, see [29] for similar approaches in computer vision. Consequently, this setup intentionally does not explicitly model a separate “remaining” class OTHER; therefore, the corresponding results table

does not include a row for the class OTHER.

External validation Model generalizability was assessed through out-of-distribution evaluation by testing on the Liu et al. dataset [5] as an external validation dataset. The external dataset contains 6 heart rhythm types, namely AF, SR, premature ventricular contraction, premature atrial contraction, VTACH, and SVTACH, which we mapped to our classification scenarios, see Table VIII in the supplementary material. It is worth noting that the external dataset is tested using the full input resolution of 1000 time steps (10 seconds). The fact that all considered model architectures involve a global average pooling layer allows for flexible input lengths at inference time, while still leveraging the model trained on *MIMIC-III-Ext-PPG*.

Subgroup analyses One of the strengths of the *MIMIC-III-Ext-PPG* dataset is the simultaneous availability of heart rhythm labels alongside other physiological parameters, including HR, BP, and demographic information. We used this information to stratify the arrhythmia detection performance by:

- 1) **BP categories** according to standard clinical guidelines [30], [31], see Table V in the supplementary material.
- 2) **HR categories** based on [32], see Table VI in the supplementary material.
- 3) Demographic/biometric categories:
 - a) **BMI categories** based on World Health Organization (WHO) recommendations [33], see Table VII.
 - b) **Ethnicity categories** were aggregated into five groups (White, Black, Asian, Hispanic, and Other), aligned with U.S. Office of Management and Budget Statistical Policy Directive No. 15 (1997) [34] and consistent with prior machine learning studies using MIMIC-III (e.g., [35]), see Table XIV.
 - c) **Gender categories** as recorded in the MIMIC-III database [36], categorized as male and female according to the structured electronic health record fields.

Performance evaluation and metrics

Regression tasks are evaluated using the Mean Absolute Error (MAE). We also assess the agree-

ment between predictions and reference values in more detail. Bland-Altman analyses were also performed [37]. We determined bias as well as the corresponding limits of agreement (LoA).

Rhythm classification performance is assessed using the area under the receiver operator characteristic curve (AUROC). To further investigate the performance of the models, we also report sensitivity while fixing the decision threshold such that we reach a specificity ≥ 0.8 , and report specificity while fixing the threshold such that sensitivity ≥ 0.80 .

III. RESULTS

A. Arrhythmia Classification Performance

As indicated in Table II, the performance of AF, SAA, and ARRH tasks for in-distribution classification is provided. In the AF task, AF detection achieved high performance for both models, with AUROC values of 0.96 for XResNet1d101 and 0.94 for LeNet1D, which translates into high sensitivity (0.92 for both models) and high specificity (0.98 vs. 0.96) at operating points of specificity/sensitivity ≥ 0.80 , respectively. AFLT detection showed lower performance, with AUROC values around 0.77–0.78, sensitivity 0.62–0.64, and specificity 0.61–0.62. In SAA, SINUS classification showed high performance for both models, where AUROC for XResNet1d101 and LeNet1D were 0.92 and 0.90, respectively, and correspondingly high values of sensitivity and specificity, where sensitivity is equal to 0.89 for XResNet1d101 and 0.86 for LeNet1D, and specificity is equal to 0.86 for XResNet1d101 and 0.84 for LeNet1D. The performance of the AF+AFLT detection remained high for both models with AUROC values of 0.95 and 0.94, sensitivity of 0.93 and 0.92, and specificity of 0.98 and 0.96 for XResNet1d101 and LeNet1D, respectively. Within the ARRH task, several rhythms showed high performance for both models, including STACH (AUROC = 0.97), SR (AUROC = 0.93), AF (AUROC = 0.94–0.96), and SBRAD (AUROC = 0.96), along with high values of sensitivity and specificity. However, some of the less common rhythms showed less performance and variability. For instance, VPACE achieved AUROC values of

0.79–0.80, compared to SARRH and JR, which showed lower AUROC and threshold metrics. Interestingly, LeNet1D showed higher performance for JR (AUROC = 0.83, sensitivity = 0.71, specificity = 0.70) compared to XResNet1d101. Overall, it is evident that XResNet1d101 showed slightly higher performance for most of the rhythms, although both models demonstrated comparable results for several classes.

B. Regression Task Performance

Table III presents the performance on all regression tasks. XResNet1d101 achieved superior performance across RR and HR prediction tasks: RR prediction with an MAE of 2.97 bpm compared to LeNet1D’s 4.53 bpm, and HR estimation with an MAE of 1.13 bpm versus 1.61 bpm for LeNet1D. In terms of BP estimation, XResNet1d101 demonstrated slightly better performance with MAEs of 16.13/8.70 mmHg (SBP/DBP) compared to LeNet1D’s 16.65/9.39 mmHg.

Furthermore, the comparative Bland–Altman analysis (model bias and LoA) for SBP, DBP, HR, and RR shows that both models have near-zero bias for all parameters. The best performance is observed for HR, where the LoAs are relatively narrow (approximately ± 8 bpm) compared with the physiological variability in the dataset (median 86.2 bpm, IQR 75.0–98.7 bpm). Performance is poorer for RR where the LoAs are wider in comparison to the physiological variability (LoAs of approximately ± 10 bpm compared to median 19.9 bpm, IQR 15.7–24.8 bpm). Performance was worst for SBP, with LoAs of approximately ± 40 mmHg, which is considerably larger than the interquartile range of SBP values in the dataset (median 121.3 mmHg, IQR 105.6–139.6 mmHg). These findings highlight that while HR estimation from PPG is highly reliable, RR estimation remains moderately challenging, and cuffless BP estimation based on PPG alone using these techniques is currently unreliable.

C. Out-of-Distribution Generalization

Figure 1 shows the out-of-distribution evaluation results for the XResNet1d101 model trained

TABLE II: In-distribution classification performance for robust AF classification (AF task), sinus versus atrial arrhythmia discrimination (SAA task), and general arrhythmia classification (ARRH task) in terms of label-dependent AUROC for the two models considered in this work.

Task	Rhythm	AUROC		Sensitivity (Specificity > 0.8)		Specificity (Sensitivity > 0.8)	
		XResNet1d101	LeNet1D	XResNet1d101	LeNet1D	XResNet1d101	LeNet1D
AF	AF	0.96	0.94	0.92	0.92	0.98	0.96
	AFLT	0.77	0.78	0.62	0.64	0.61	0.62
SAA	SINUS	0.92	0.90	0.89	0.86	0.86	0.84
	AF+AFLT	0.95	0.94	0.93	0.92	0.98	0.96
ARRH	SR	0.93	0.93	0.93	0.92	0.89	0.89
	STACH	0.97	0.97	0.97	0.97	0.97	0.97
	AF	0.96	0.94	0.94	0.92	0.96	0.96
	SBRAD	0.96	0.96	0.95	0.95	0.98	0.98
	VPACE	0.79	0.80	0.62	0.64	0.60	0.63
	AVPACE	0.89	0.87	0.81	0.76	0.81	0.77
	AFLT	0.78	0.78	0.65	0.64	0.60	0.60
	APACE	0.80	0.78	0.63	0.60	0.61	0.57
	SARRH	0.61	0.66	0.40	0.49	0.26	0.27
	JR	0.62	0.83	0.45	0.71	0.20	0.70
	SVTACH	0.78	0.68	0.65	0.60	0.54	0.57
	MATACH	0.84	0.78	0.72	0.70	0.72	0.60
VTACH	0.75	0.63	0.60	0.33	0.49	0.40	

TABLE III: Regression performance including MAE, Bland–Altman bias, and 95% limits of agreement (LoA) for BP, HR, and RR obtained with a median baseline predictor, XResNet1d101, and LeNet1D.

Parameter	Baseline	XResNet1d101			LeNet1D		
	MAE	MAE	Bias	95% LoA	MAE	Bias	95% LoA
SBP [mmHg]	19.06	16.13	-2.58	[-43.16, 38.00]	16.65	-1.24	[-43.00, 40.52]
DBP [mmHg]	10.09	8.70	0.79	[-21.34, 22.92]	9.39	2.53	[-20.38, 25.45]
HR [bpm]	14.37	1.13	-0.14	[-8.00, 7.72]	1.61	0.03	[-8.77, 8.84]
RR [bpm]	5.34	2.97	-0.17	[-10.07, 9.72]	4.53	0.31	[-11.89, 12.50]

on *MIMIC-III-Ext-PPG* and tested on the external dataset by Liu et al [5], [38]. It is worth recalling that, since the external dataset lacks several rhythm classes found in *MIMIC-III-Ext-PPG*, our results are limited to the shared classes such as AF, SR, SVTACH, and VTACH.

The AF task scenario demonstrated exceptional cross-dataset transferability with an AUROC of 0.97 for AF detection, in line with the strong in-distribution performance (AUROC 0.96) and confirming the robustness of PPG-based AF detection algorithms across different patient populations

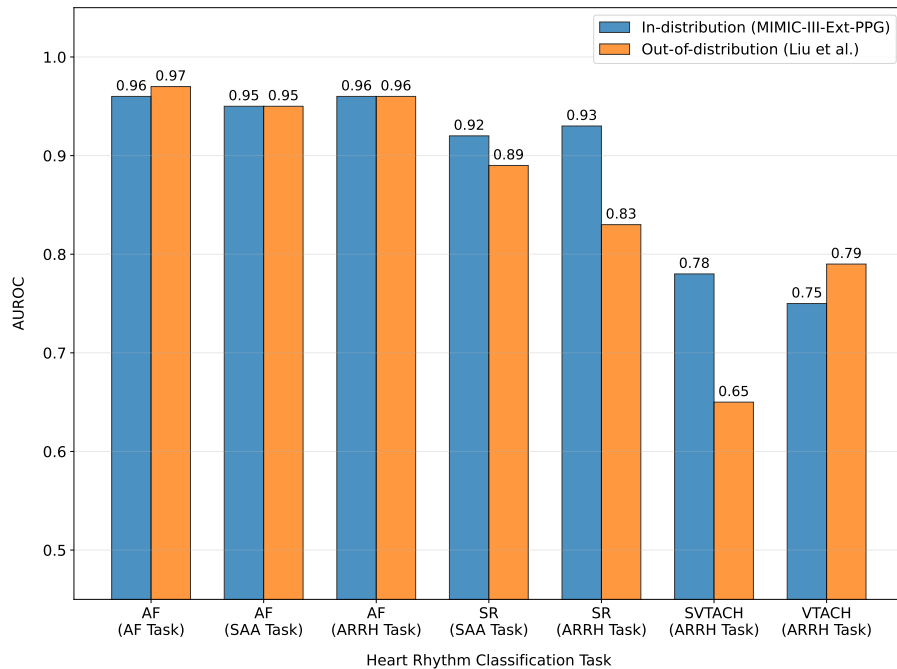


Fig. 1: External validation of the rhythm classification performance (using XResNet1d101) demonstrating robust generalization of PPG-based rhythm classification, with AF detection showing exceptional cross-dataset transferability.

and recording conditions. Similarly, the SAA task demonstrated strong generalization for atrial arrhythmia detection (AUROC of 0.95 vs. internal AUROC 0.95) and slightly worsened discrimination for SR detection (AUROC of 0.89 vs. internal AUROC 0.92) for the external dataset. For the arrhythmia classification (ARRH task), the XResNet1d101 model retains high performance for AF detection (AUROC 0.96 vs. internal AUROC 0.96). However, a notable degradation in performance is seen for SR classification (AUROC 0.83 vs. internal AUROC 0.93). A slight improvement in performance is seen for VTACH (AUROC 0.79 vs. internal AUROC 0.75), but for SVTACH (AUROC 0.65 vs. internal AUROC 0.78), the model performs significantly worse on the external dataset. One possible explanation for the drop in SR detection performance in the ARRH scenario could be the fact that the model predicts four finegrained SR subclasses, but

is evaluated only on a coarse SR class in the external dataset. This result is in line with the strong external validation result for the coarse SR class (AUROC 0.89) for the SAA task.

D. Subgroup Analyses

In this section, we analyzed the arrhythmia classification performance (all three tasks) of the XResNet1d101 model stratified by BP, HR, gender, BMI, and ethnicity categories (when available).

Stratification according to BP Tables X and XI summarize rhythm classification performance across BP categories. In the AF task, the performance of the AF detection method is consistently high across BP groups with AUROC values between 0.95 and 0.99, coupled with high sensitivity (0.92–0.99) and specificity (0.98–1.00). In the case of AFLT detection, the performance is lower and shows moderate variability across BP groups, with

AUROC values ranging from 0.77 to 0.84 and corresponding sensitivity and specificity values between 0.54–0.78 and 0.65–0.79, respectively. In the SAA task, SINUS classification achieved AUROC values between 0.88 and 0.97, while AF+AFLT detection was high and stable across BP groups (0.96–0.99) with high sensitivity and specificity. For the ARRH task, common rhythms such as SR (0.92–0.96), STACH (0.96–0.98), and AF (0.95–0.99) had a stable performance across all BP groups. On the other hand, several less common rhythms had a less stable performance across the BP groups, such as VPACE (0.65–0.91), SVTACH (0.47–0.93), and VTACH (0.42–0.92), which was also reflected in more variable sensitivity and specificity values.

Stratification according to HR Tables X and XI present the performance of the rhythm classification algorithms across HR categories. In the AF task, the performance of AF detection increased with the increase of HR. The AUROC of AF detection increased from 0.88 in the bradycardia category to 0.97 in the tachycardia category. Meanwhile, the sensitivity and specificity of AF detection increased from 0.79 / 0.78 to 0.96 / 0.97. In the AFLT detection task, the AUROC of AFLT detection increased from 0.74 to 0.86. Meanwhile, the sensitivity and specificity of AFLT detection increased from 0.51 / 0.50 to 0.73 / 0.76. In the SAA task, SINUS classification improved from 0.84 AUROC in bradycardia to 0.96 in tachycardia, with corresponding increases in sensitivity and specificity (0.70 / 0.74 vs. 0.97 / 0.95), while AF+AFLT detection remained consistently strong (0.87–0.97 AUROC). Within the ARRH task, several rhythms showed reduced performance in bradycardia, such as SR (0.72 AUROC, 0.51 / 0.49 sensitivity/specificity). In contrast, some rhythms showed improved performance at higher HR values, including APACE (0.96 AUROC, 0.97 / 0.96 sensitivity/specificity).

Stratification according to gender Table XII shows AUROC scores stratified according to gender, BMI and ethnicity, see Table XIII for corresponding sensitivity/specificity metrics. Across gender groups, rhythm classification performance remained largely comparable. In the AF task, AF detection achieved similar AUROC values in females

and males (0.95 vs. 0.96) with nearly identical sensitivity and specificity (0.92/0.98 vs. 0.93/0.98). AFLT detection showed moderate variation (0.84 vs. 0.75 AUROC, 0.74/0.74 vs. 0.60/0.59 sensitivity/specificity). In the SAA task, both SINUS (0.91 vs. 0.93) and AF+AFLT (0.95 vs. 0.95) detection remained consistent across genders with comparable threshold metrics. Within the ARRH task, most common rhythms also showed similar performance (e.g., SR 0.93 vs. 0.92, STACH 0.97 vs. 0.97), although some rhythms exhibited moderate variation such as VPACE (0.71 vs. 0.84 AUROC).

Stratification according to BMI Moderate differences were observed across BMI groups. In the AF task, AF detection increased from 0.92 AUROC in normal BMI to 0.98 in obese subjects, with sensitivity/specificity increasing from 0.89/0.94 to 0.97/0.99. AFLT detection remained relatively stable (0.72–0.75 AUROC). In the SAA task, SINUS classification improved from 0.84 (normal BMI) to 0.96 (obese) with corresponding increases in sensitivity and specificity (0.69/0.72 vs. 0.97/0.94), while AF+AFLT detection remained high across BMI groups (0.93–0.97 AUROC). Similar trends were observed for several ARRH rhythms such as SR (0.87–0.95 AUROC) and VPACE (0.65–0.95 AUROC).

Stratification according to ethnicity For all ethnicity groups, most of the rhythms demonstrated comparable performance. In the AF task, the AUROC of AF detection varied from 0.95 to 0.98, with high sensitivity and specificity (e.g., 0.90/0.97 in the White ethnicity, 0.96/0.99 in the Asian ethnicity). In the SAA task, the AUROC of SINUS classification varied from 0.82 to 0.98, while the AUROC of AF+AFLT detection was stable at 0.95 to 0.98. Within the ARRH task, common rhythms such as SR (0.91–0.98) and STACH (0.97–0.99) showed stable performance across ethnic groups, while some less frequent rhythms showed larger variability.

IV. DISCUSSION

Heart Rhythm Classification Performance Our comprehensive benchmarking establishes the performance baselines for PPG-based clinical predic-

tion tasks on the recently published *MIMIC-III-Ext-PPG* dataset. The strong performance in AF detection (AUROC ≈ 0.95) confirms the clinical utility of the PPG for the most common arrhythmia detection application in a large and diverse ICU population. Similarly, the SAA task achieved consistently high in-distribution performance (AUROC $\sim 0.92 - 0.95$), supporting reliable discrimination between sinus rhythms and atrial arrhythmias using PPG alone. Compared to other state-of-the-art AF classification studies, the advantages of leveraging our large, diverse dataset with high AUROC, even in the challenging ICU setting, are clear. While high AUROC ($\sim 0.99-1.0$) is often achieved on limited cohorts (e.g., $N < 50$ in [39]–[41]) or ambulatory data, performance often drops significantly when scaling up (e.g., AUROC 0.72 in [42]). Furthermore, [16] on the DeepBeat dataset [43] reported AUROC in the $\sim 0.8-0.9$ range with less than 200 patients. Our results (AUROC ≈ 0.95) on a large and diverse clinical population (up to 6,189 patients, 53,331 hours of data) demonstrate superior robustness in a real-world ICU environment.

Most notably, this is the first work that systematically explores the prospects of PPG for general arrhythmia detection, demonstrating the applicability of PPG-based heart rhythm analysis beyond AF/AFLT. We believe that the currently moderate overall performance highlights the inherent challenges in extracting complex electrophysiological information from peripheral pulse morphology alone and should be seen as a challenging benchmark for the community. We also deliberately left the small classes, e.g., VTACH or JR, in the dataset, for which classification performance remained limited, to encourage future methodological advances targeting these clinically important but difficult arrhythmias.

Regression performance The regression task results give valuable insights into PPG’s quantitative monitoring potential. HR estimation accuracy (MAE 1.13-1.61 bpm) outperforms recent state-of-the-art approaches, including Q-PPG’s 4.41 bpm [44] and EnhancePPG’s 3.54 bpm [45], and also demonstrates superior performance compared to methods achieving 1.86-3.78 bpm under motion

artifact conditions [46]. The RR prediction model demonstrated an MAE of 2.97-4.53 bpm, which is competitive with recent approaches, including deep learning models reporting 2.0-3.13 bpm [47], [48], indicating performance characteristics that warrant investigation for ICU monitoring applications. For BP estimation, our models achieved MAE of 16.13-16.65 mmHg for SBP and 8.70-9.39 mmHg for DBP (Table IX). While our DBP performance is comparable to other MIMIC-III subset benchmarks (e.g., [10], [49] reported $\sim 9-10$ mmHg), our SBP MAE falls within, but toward the upper bound of their reported range ($\sim 13-17$ mmHg). Finally, all model comparisons that do not rely on an identical dataset and splits have to be taken with a grain of salt. Furthermore, Table III reveals substantial variability in BP estimation, with particularly wide LoA ranges for SBP and DBP, indicating large per-sample fluctuations despite low average error. This trend is also observed in [10], which used the ICU PPG data for BP prediction. The main conclusion on BP estimation seems to be that a larger dataset does not lead to a substantial reduction of BP prediction errors. Therefore, BP estimation from PPG alone remains a challenging use case.

Architecture Comparison and Model Selection The comparable performance between XResNet1d101 and LeNet1D across most tasks indicates that PPG signal features may not require the depth in architecture that is commonly necessary for image recognition tasks. While XResNet1d101 achieved slightly higher performance in AF detection, LeNet1D demonstrated competitive performance with a substantially simpler architecture, and showed slightly superior performance in BP estimation, indicating that simpler models may actually be advantageous for certain PPG applications, potentially offering better generalization and computational efficiency [16]. The minimal performance differences between architectures also indicate that data quality and preprocessing may be more critical factors than model complexity for PPG applications.

Out-of-Distribution Generalization Overall, the external validation results indicate excellent generalization capabilities of the rhythm classification models, showing good agreement between the

performance levels achieved on internal and external datasets. The most striking deterioration in external vs. internal model performance occurred for supraventricular tachycardia, where already the internal model performance is not outstanding. As SVTACH is one of the least populated rhythm types, we see it as very likely that the model performance could improve with more training data.

Stratification according to BP The BP stratification analysis indicates that rhythm classification performance remains largely stable across blood pressure categories for the principal rhythms. AF detection maintained consistently high. Similar robustness was observed for AF+AFLT detection in the SAA task, suggesting that the learned representations for atrial rhythm irregularity are largely preserved across different hemodynamic states. In contrast, several less frequent arrhythmias showed greater variability across BP strata. Rhythms such as VPACE, SVTACH, and VTACH exhibited larger fluctuations in AUROC as well as sensitivity and specificity values across BP groups. This variability may reflect both the smaller number of available samples for these rhythms and the physiological effects of blood pressure on peripheral pulse characteristics. Variations in vascular tone and arterial stiffness associated with different blood pressure states are known to alter the morphology and timing characteristics of the PPG waveform [1], which may contribute to increased classification variability for rhythm types with more subtle waveform patterns. Overall, these results suggest that BP variations have a limited influence on the detection of dominant rhythms such as AF and SR, while rarer arrhythmias may be more sensitive to physiological variability and dataset imbalance.

Stratification according to HR The HR subgroup analysis showed more differentiated performance differences than those observed across BP categories. The performance in AF detection improved with increasing heart rate (AUROC increasing from 0.88 in bradycardia to 0.97 in tachycardia). These improvements in performance were also found for AFLT and SINUS detection, indicating that higher heart rates facilitate clearer discrimination of atrial rhythm irregularities. However, several rhythms

showed reduced performance in bradycardic segments. For instance, SR classification performance decreased in bradycardia, and for STACH, specificity was significantly decreased in bradycardia. These findings imply that lower heart rates may reduce the distinctiveness of temporal rhythm patterns in PPG signals. These findings are consistent with prior studies showing that heart rate strongly affects PPG waveform morphology and rhythm detectability. AF detection algorithms commonly rely on irregular pulse-to-pulse intervals derived from PPG signals. In AF, these intervals become highly variable compared to the regular spacing observed in SR, providing an important cue for rhythm classification [50]. In summary, the proposed HR stratification results emphasize the importance of the heart rate as a significant factor for PPG waveform rhythm classification performance.

Stratification according to gender The gender-based analysis revealed largely comparable rhythm classification performance between female and male subjects, which is an important indicator of algorithmic fairness across sex groups. AF detection achieved similar AUROC values across genders (0.95 vs. 0.96) with nearly identical sensitivity and specificity, suggesting that the model generalizes well across sex-related physiological differences. Moderate variations were observed for certain rhythms such as AFLT and VPACE. These differences may reflect known sex-related variations in cardiovascular physiology and peripheral pulse morphology, which can influence PPG waveform characteristics [51]. Overall, the small differences observed between genders indicate that the proposed model maintains fair and robust rhythm classification performance across sexes, consistent with recommendations for equitable medical AI systems [52]

Stratification according to BMI The BMI-based analysis revealed moderate performance differences across body composition groups. In particular, AF and SINUS detection showed improved performance in obese subjects compared with normal BMI groups. These findings may reflect the influence of body composition on peripheral pulse characteristics and vascular dynamics. Previous studies

have shown that obesity can alter arterial stiffness and pulse wave propagation dynamics [53], [54], which may influence peripheral pulse characteristics and consequently the discriminative features learned from PPG signals. Nevertheless, the overall classification performance remained high across BMI categories, indicating robust model generalization.

Stratification according to ethnicity The ethnicity-based analysis showed broadly consistent rhythm classification performance across ethnic groups. For example, AF detection remained stable across White, Black, Asian, and Hispanic groups (AUROC 0.95–0.98) with similarly high sensitivity and specificity. These findings suggest that the learned rhythm representations generalize well across demographic groups in the dataset. This observation is consistent with the results in [55], which did not observe significant differences in PPG beat detection on the MIMIC dataset between Black and White subjects. However, it is in stark contrast to [56], where pulse oximetry was found to be less accurate in Black compared to White subjects. This could be explained by the analyses in the present study and Charlton et al [55] using single-channel PPG, whereas pulse oximetry [56] uses dual-channel PPG, potentially making it more susceptible to racial bias. In addition, taking into consideration these interactions, model calibration or cost-sensitive training could potentially help in reducing deployment biases.

Limitations and Future Directions Several limitations warrant consideration. First, our observation is limited to ICU patients, whose pathophysiology may limit generalizability to ambulatory or healthy populations. Also, the use of the 30-second segment length, while suitable for rhythm classification, may be insufficient for detecting paroxysmal arrhythmias or capturing long-term hemodynamic trends. Furthermore, our work is based solely on the PPG signal, which is restrictive from the application point of view, as motion artifacts cause severe signal distortion in real-world cases.

Future research should prioritize several key areas: (1) development of BP-adaptive algorithms to address the performance variability under different hemodynamic states; (2) multi-modal fusion strate-

gies combining PPG with other readily available signals and/or static patient metadata; (3) prospectively conducted clinical trials for assessment of efficacy and safety for deployment in the field; and (4) integration of simultaneous accelerometry signals and advanced techniques, including the TROIKA algorithm [57], to detect heart rates and rhythms under motion conditions.

V. SUMMARY AND CONCLUSION

This study establishes a benchmarking framework for PPG-based clinical prediction, providing comprehensive performance baselines across both classification and regression tasks using the *MIMIC-III-Ext-PPG* dataset. Our rigorous evaluation of 6.3 million PPG segments in 6,189 ICU patients illustrates the possibility of multi-task physiological monitoring by a single biosignal. Regression performance revealed strong results for respiratory rate estimation, but in particular heart rate estimation and confirmed the challenging case of blood pressure prediction from PPG alone. For arrhythmia detection, we demonstrated strong performance on different application scenarios such as atrial fibrillation detection (AF) and sinus versus atrial arrhythmia discrimination (SAA). Most notably, however, this work provides the first comprehensive assessment of PPG-based general arrhythmia classification (ARRH) across 13 finegrained classes. All models achieved strong performance for common rhythms such as AF, SR, STACH, and SBRAD, with AUROC values generally above 0.93 and consistently high sensitivity and specificity with robust performance in external validation and in subgroup analyses. We hope that the presented analysis can serve as a starting point and inspiration for more detailed assessments of PPG-based prediction problems.

Overall, these results provide a comprehensive reference baseline for PPG-based physiological monitoring and demonstrate the potential of deep learning models to extract a range of clinically relevant information from a single biosignal. Future research should prioritize BP-adaptive algorithms, multi-modal fusion approaches, and prospective clinical validation studies. The established baselines

provide a foundation for regulatory approval pathways and clinical integration strategies.

CODE AVAILABILITY

This work is exclusively based on publicly available datasets. The datasets underlying this study are publicly available [5], [20]. The source code underlying our investigations is available at https://github.com/AI4HealthUOL/MIMIC-III-Ext-PPG_benchmarking.

ACKNOWLEDGMENTS

The project (22HLT01 QUMPHY) has received funding from the European Partnership on Metrology, co-financed from the European Union's Horizon Europe Research and Innovation Programme and by the Participating States. Funding for NPL and the University of Cambridge was provided by Innovate UK under the Horizon Europe Guarantee Extension, grant numbers 10084125 and 10091955. PHC acknowledges funding from the British Heart Foundation (BHF) grant [FS/20/20/34626].

COMPETING INTERESTS

PHC performs consultancy work for wearable manufacturers who use PPG sensors in their products; however, none of these companies had any influence on the conception or realization of this study. The other authors declare no competing interests.

REFERENCES

- [1] J. Allen, "Photoplethysmography and its application in clinical physiological measurement," *Physiological Measurement*, vol. 28, no. 3, p. R1, 2007.
- [2] P. H. Charlton, D. A. Birrenkott, T. Bonnici, M. A. Pimentel, A. E. Johnson, J. Alastruey, L. Tarassenko, P. J. Watkinson, R. Beale, and D. A. Clifton, "Wearable photoplethysmography for cardiovascular monitoring," *Proceedings of the IEEE*, vol. 110, no. 3, pp. 355–381, 2022.
- [3] M. Elgendi, "Standard terminologies for photoplethysmogram signals," *Current Cardiology Reviews*, vol. 8, no. 3, pp. 215–219, 2012.
- [4] D. Castaneda, A. Esparza, M. Ghamari, C. Soltanpur, and H. Nazeran, "A review on wearable photoplethysmography sensors and their potential future applications in health care," *International Journal of Biosensors & Bioelectronics*, vol. 4, no. 4, p. 195, 2018.
- [5] Z. Liu, B. Zhou, Z. Jiang, X. Chen, Y. Li, M. Tang, and F. Miao, "Multiclass arrhythmia detection and classification from photoplethysmography signals using a deep convolutional neural network," *Journal of the American Heart Association*, vol. 11, no. 7, p. e023555, 2022.
- [6] J. Torres-Soto and E. A. Ashley, "Multi-task deep learning for cardiac rhythm detection in wearable devices," *NPJ Digital Medicine*, vol. 3, no. 1, pp. 1–12, 2020.
- [7] M. Moulaeifard, L. Coquelin, M. Rinkevicius, A. Sološenko, O. Pfeffer, C. Bench, N. Hegemann, S. Vardanega, M. Nandi, J. Alastruey, C. Heiss, V. Marozas, A. Thompson, P. J. Aston, P. H. Charlton, and N. Strodthoff, "Machine-learning for photoplethysmography analysis: Benchmarking feature, image, and signal-based approaches," *Biomedical Signal Processing and Control*, vol. 120, p. 109831, 2026. [Online]. Available: <https://www.sciencedirect.com/science/article/pii/S174680942600385X>
- [8] A. Gaurav, M. Maheedhar, V. R. Tiwari, and R. Narayanan, "Cuff-less PPG based continuous blood pressure monitoring—A smartphone based approach," in *2016 38th Annual International Conference of the IEEE Engineering in Medicine and Biology Society (EMBC)*. IEEE, 2016, pp. 607–610.
- [9] X. Ding, B. P. Yan, Y.-T. Zhang, J. Liu, N. Zhao, and H. K. Tsang, "Continuous cuffless blood pressure estimation using pulse transit time and photoplethysmogram intensity ratio," *IEEE Transactions on Biomedical Engineering*, vol. 63, no. 5, pp. 964–972, 2016.
- [10] M. Moulaeifard, P. H. Charlton, and N. Strodthoff, "Generalizable deep learning for photoplethysmography-based blood pressure estimation—A benchmarking study," *Machine Learning: Health*, 2025.
- [11] W. Karlen, S. Raman, J. M. Ansermino, and G. A. Dumont, "Multiparameter respiratory rate estimation from the photoplethysmogram," *IEEE Transactions on Biomedical Engineering*, vol. 60, no. 7, pp. 1946–1953, 2013.
- [12] P. S. Addison, J. N. Watson, M. L. Mestek, J. P. Ochs, A. A. Uribe, and S. D. Bergese, "Pulse oximetry-derived respiratory rate in general care floor patients," *Journal of Clinical Monitoring and Computing*, vol. 29, no. 1, pp. 113–120, 2015.
- [13] P. H. Charlton, T. Bonnici, L. Tarassenko, D. A. Clifton, R. Beale, and P. J. Watkinson, "An assessment of algorithms to estimate respiratory rate from the electrocardiogram and photoplethysmogram," *Physiological Measurement*, vol. 37, no. 4, p. 610, 2016.
- [14] M. A. Pimentel, A. E. Johnson, P. H. Charlton, D. Birrenkott, P. J. Watkinson, L. Tarassenko, and D. A. Clifton, "Toward a robust estimation of respiratory rate from pulse oximeters," *IEEE Transactions on Biomedical Engineering*, vol. 64, no. 8, pp. 1914–1923, 2016.
- [15] M. Sicbaldi, L. Palmerini, S. Moscato, P. di Florio, A. Silvani, and L. Chiari, "Benchmarking of open-source algorithms for heart rate estimation from motion-corrupted photoplethysmography," *Computers in Biology and Medicine*, vol. 196, p. 110808, 2025.
- [16] M. Moulaeifard, L. Coquelin, M. Rinkevicius, A. Sološenko, O. Pfeffer, C. Bench, N. Hegemann, S. Vardanega, M. Nandi, J. Alastruey *et al.*, "Machine-learning for photoplethysmography analysis:

- Benchmarking feature, image, and signal-based approaches,” *arXiv preprint arXiv:2502.19949*, 2025.
- [17] L. F. Polanía, L. K. Mestha, D. T. Huang, and J.-P. Couderc, “Method for classifying cardiac arrhythmias using photoplethysmography,” in *2015 37th Annual International Conference of the IEEE Engineering in Medicine and Biology Society (EMBC)*. IEEE, 2015, pp. 6574–6577.
- [18] D. Han, S. K. Bashar, F. Mohagheghian, E. Ding, C. Whitcomb, D. D. McManus, and K. H. Chon, “Premature atrial and ventricular contraction detection using photoplethysmographic data from a smartwatch,” *Sensors*, vol. 20, no. 19, p. 5683, 2020.
- [19] L. Jeanningros, J. Van Zaen, M. Le Bloa, C. Teres, C. Herrera, A. Porretta, G. Domenichini, P. Pascale, A. Luca, J. Solana Munoz *et al.*, “Non-invasive detection of cardiac arrhythmias using photoplethysmography signals,” *Europace*, vol. 26, no. Supplement_1, pp. euae102–674, 2024.
- [20] M. Moulaeifard, P. H. Charlton, and N. Strodthoff, “MIMIC-III-Ext-PPG: A PPG Benchmark Dataset for Cardiorespiratory Analysis (Version 1.1.0),” *PhysioNet*, <https://doi.org/10.13026/r6k1-xt76>, Mar. 2026.
- [21] A. L. Goldberger, L. A. N. Amaral, L. Glass, J. M. Hausdorff, P. C. Ivanov, R. G. Mark, J. E. Mietus, G. B. Moody, C.-K. Peng, and H. E. Stanley, “PhysioBank, PhysioToolkit, and PhysioNet,” *Circulation*, vol. 101, no. 23, pp. e215–e220, 2000.
- [22] B. Moody, G. Moody, M. Villarroel, G. Clifford, and I. Silva, “MIMIC-III waveform database matched subset,” *PhysioNet*, <https://doi.org/10.13026/c2294b>, 2020.
- [23] N. Strodthoff, P. Wagner, T. Schaeffter, and W. Samek, “Deep learning for ECG analysis: Benchmarks and insights from PTB-XL,” *IEEE Journal of Biomedical and Health Informatics*, vol. 25, no. 5, pp. 1519–1528, 2021.
- [24] P. Wagner, T. Mehari, W. Haverkamp, and N. Strodthoff, “Explaining deep learning for ecg analysis: Building blocks for auditing and knowledge discovery,” *Computers in Biology and Medicine*, vol. 176, p. 108525, Jun. 2024.
- [25] D. Makowski, T. Pham, Z. J. Lau, J. C. Brammer, F. Lespinasse, H. Pham, C. Schölzel, and S. A. Chen, “NeuroKit2: A Python toolbox for neurophysiological signal processing,” *Behavior Research Methods*, vol. 53, pp. 1–8, 2021.
- [26] I. Loshchilov and F. Hutter, “Decoupled weight decay regularization,” *arXiv preprint arXiv:1711.05101*, 2017. [Online]. Available: <https://arxiv.org/abs/1711.05101>
- [27] Z. Xiao *et al.*, “Advancing cuffless blood pressure estimation: A PPG-based multi-task learning approach,” *Future Generation Computer Systems*, vol. 107, p. 107689, 2024. [Online]. Available: <https://www.sciencedirect.com/science/article/abs/pii/S1746809424004361>
- [28] M. Moulaeifard, P. H. Charlton, and N. Strodthoff, “Generalizable deep learning for photoplethysmography-based blood pressure estimation—A benchmarking study,” *Machine Learning: Health*, vol. 1, no. 1, p. 010501, Sep. 2025. [Online]. Available: <http://dx.doi.org/10.1088/3049-477X/ae01a8>
- [29] R. Wightman, H. Touvron, and H. Jegou, “ResNet strikes back: An improved training procedure in timm,” in *NeurIPS 2021 Workshop on ImageNet: Past, Present, and Future*, 2021.
- [30] J. M. Flack and B. Adekola, “Blood pressure and the new ACC/AHA hypertension guidelines,” *Trends in Cardiovascular Medicine*, vol. 30, no. 3, pp. 160–164, 2020.
- [31] S. Sharma, M. F. Hashmi, and P. T. Bhattacharya, “Hypotension,” in *StatPearls [internet]*. StatPearls Publishing, 2023.
- [32] F. M. Kusumoto *et al.*, “Part 7.3: Management of symptomatic bradycardia and tachycardia: 2005 American Heart Association guidelines for cardiopulmonary resuscitation and emergency cardiovascular care,” *Circulation*, vol. 112, no. 24_suppl, pp. IV–67–IV–77, 2005.
- [33] W. H. Organization, *Obesity: Preventing and Managing the Global Epidemic*, ser. WHO Technical Report Series. Geneva: World Health Organization, 2000, vol. 894.
- [34] O. of Management and Budget, “Revisions to the standards for the classification of federal data on race and ethnicity,” *Federal Register*, vol. 62, no. 210, pp. 58 782–58 790, 1997.
- [35] J. Chen, I. Berlot-Attwell, X. Wang, S. Hossain, and F. Rudzicz, “Exploring text specific and blackbox fairness algorithms in multimodal clinical nlp,” in *Proceedings of the 3rd Clinical Natural Language Processing Workshop*, 2020, pp. 301–312.
- [36] A. Johnson, T. Pollard, and R. Mark, “MIMIC-III Clinical Database (version 1.4),” *PhysioNet*, <https://doi.org/10.13026/C2XW26>, 2019.
- [37] J. M. Bland and D. Altman, “Statistical methods for assessing agreement between two methods of clinical measurement,” *The Lancet*, vol. 327, no. 8476, pp. 307–310, 1986.
- [38] S. Bashar, “Atrial fibrillation annotations of electrocardiogram from mimic iii matched subset,” *figshare*, 2020. [Online]. Available: <https://doi.org/10.6084/m9.figshare.12149091.v1>
- [39] A. Aliamiri and J. Shen, “A recurrent neural network for atrial fibrillation detection using photoplethysmography,” *Conference Proceedings, IEEE BSN*, 2018.
- [40] S. Gotlibovych *et al.*, “CNN-based approach for atrial fibrillation detection from short-term PPG signals,” *Conference Proceedings, IEEE EMBC*, 2018.
- [41] S. Nemati *et al.*, “A robust algorithm for detecting atrial fibrillation using wearable devices,” *IEEE Journal of Biomedical and Health Informatics*, vol. 20, no. 6, pp. 1550–1560, 2016.
- [42] G. Tison *et al.*, “Passive detection of atrial fibrillation using a wrist-worn consumer device: The Apple Heart Study,” *The New England Journal of Medicine*, vol. 379, no. 18, pp. 1707–1716, 2018.
- [43] J. Torres-Soto and E. A. Ashley, “Multi-task deep learning for cardiac rhythm detection in wearable devices,” *NPJ Digital Medicine*, vol. 3, no. 1, p. 116, 2020.
- [44] A. Burrello, D. Jahier Pagliari, M. Risso, S. Benatti, E. Macii, L. Benini, and M. Poncino, “Q-PPG: Energy-efficient PPG-based heart rate monitoring on wearable devices,” *IEEE Transactions on Biomedical Circuits and Systems*, vol. 15, no. 6, pp. 1196–1209, 2021.
- [45] A. Burrello *et al.*, “EnhancePPG: Improving PPG-based heart rate estimation with self-supervision and augmentation,” *arXiv preprint arXiv:2412.17860*, December 2024, available at: <https://arxiv.org/abs/2412.17860>.
- [46] S. Thakur, P. C.-P. Chao, and C.-H. Tsai, “Precision heart rate estimation using a PPG sensor patch equipped with

- new algorithms of pre-quality checking and hankel decomposition,” *Sensors*, vol. 23, no. 13, p. 6180, July 2023.
- [47] W. J. Chin, B.-H. Kwan, W. Y. Lim, Y. K. Tee, S. Dar-maraju, H. Liu, and C.-H. Goh, “A novel respiratory rate estimation algorithm from photoplethysmogram using deep learning model,” *Diagnostics*, vol. 14, no. 3, p. 284, January 2024.
- [48] J. Yu, Y.-J. Sim, S.-H. Kang, J. Ryu, S. Y. Cho, and T.-Y. Heo, “Evaluation of the photoplethysmogram-based deep learning model for continuous respiratory rate estimation in surgical intensive care unit,” *Sensors*, vol. 23, no. 20, p. 8575, October 2023.
- [49] I. Sanches, V. V. Gomes, C. Caetano, L. S. Cabrera, V. H. Cene, T. Beltrame, W. Lee, S. Baek, and O. A. Penatti, “MIMIC-BP: A curated dataset for blood pressure estimation,” *Scientific Data*, vol. 11, no. 1, p. 1233, 2024.
- [50] T. Pereira, N. Tran, K. Gadhoumi, M. M. Pelter, D. H. Do, R. J. Lee, R. Colorado, K. Meisel, and X. Hu, “Photoplethysmography based atrial fibrillation detection: a review,” *NPJ digital medicine*, vol. 3, no. 1, p. 3, 2020.
- [51] S. Dehghanojamahalleh and M. Kaya, “Sex-related differences in photoplethysmography signals measured from finger and toe,” *IEEE journal of translational engineering in health and medicine*, vol. 7, pp. 1–7, 2019.
- [52] L. Seyyed-Kalantari, H. Zhang, M. B. McDermott, I. Y. Chen, and M. Ghassemi, “Underdiagnosis bias of artificial intelligence algorithms applied to chest radiographs in under-served patient populations,” *Nature medicine*, vol. 27, no. 12, pp. 2176–2182, 2021.
- [53] N. Nordstrand, E. Gjevestad, K. Dinh, D. Hofsø, J. Røislien, and et al., “The relationship between various measures of obesity and arterial stiffness in morbidly obese patients,” *Atherosclerosis*, vol. 219, no. 2, pp. 547–552, 2011.
- [54] K. Petersen, N. Blanch, J. Keogh, and P. Clifton, “Effect of weight loss on pulse wave velocity: A systematic review and meta-analysis,” *Obesity Reviews*, vol. 16, no. 11, pp. 994–1006, 2015.
- [55] P. H. Charlton, K. Kotzen, E. Mejía-Mejía, P. J. Aston, K. Budidha, J. Mant, C. Pettit, J. A. Behar, and P. A. Kyriacou, “Detecting beats in the photoplethysmogram: benchmarking open-source algorithms,” *Physiological Measurement*, vol. 43, no. 8, p. 085007, 2022.
- [56] M. W. Sjoding, R. P. Dickson, T. J. Iwashyna, S. E. Gay, and T. S. Valley, “Racial bias in pulse oximetry measurement,” *New England Journal of Medicine*, vol. 383, no. 25, pp. 2477–2478, 2020.
- [57] Z. Zhang, Z. Pi, and B. Liu, “Troika: A general framework for heart rate monitoring using wrist-type photoplethysmographic signals during intensive physical exercise,” *IEEE Transactions on Biomedical Engineering*, vol. 62, no. 2, pp. 522–531, 2014.
- [58] P. K. Whelton, R. M. Carey, W. S. Aronow, D. E. Casey, K. J. Collins, C. Dennison Himmelfarb, S. M. DePalma, S. Gidding, K. A. Jamerson, D. W. Jones *et al.*, “2017 ACC/AHA/AAPA/ABC/ACPM/AGS/APhA/ASH/ASPC/NMA/PCNA guideline for the prevention, detection, evaluation, and management of high blood pressure in adults: A report of the American College of Cardiology/American Heart Association Task Force on Clinical Practice Guidelines,” *Journal of the American College of Cardiology*, vol. 71, no. 19, pp. e127–e248, 2018.
- [59] W. Wang, P. Mohseni, K. L. Kilgore, and L. Najafizadeh, “PulseDB: A large, cleaned dataset based on MIMIC-III and VitalDB for benchmarking cuff-less blood pressure estimation methods,” *Frontiers in Digital Health*, vol. 4, p. 1090854, 2023.

APPENDIX A
SUPPLEMENTARY TABLES

APPENDIX

This appendix provides supplementary information related to the dataset construction, clinical categorization criteria, external dataset mappings, and detailed subgroup performance analyses.

- Table IV summarizes the mapping of heart rhythm annotations after applying patient and sample threshold rules, as well as their assignment across the three classification tasks used in this study.
- Tables V and VI present the clinical criteria used to categorize blood pressure (BP) and heart rate (HR), respectively. Table VII summarizes the body mass index (BMI) categories based on WHO guidelines.
- Table VIII describes the mapping between rhythm labels used in the Liu et al. dataset and the classification tasks defined in this work. Table IX provides a comparison of BP estimation performance with previously published studies using MIMIC-III-derived datasets.
- Tables X and XI report detailed rhythm classification performance across BP and HR physiological categories.
- Tables XII and XIII present subgroup analyses across demographic factors, including gender, BMI, and ethnicity.
- Table XIV lists the mapping of original MIMIC-III ethnicity labels into aggregated demographic groups used in the fairness and subgroup analyses.

TABLE IV: Rhythm mapping after applying sample and patient threshold rules. OTHER is not considered as a separate class, but samples are retained with zero labels for all outputs to improve robustness to non-target rhythms.

Rhythm	Description	Patients	Samples (30s)	Rhythm per Tasks (mapped)		
				AF (Task 1)	SAA (Task 2)	ARRH (Task 3)
SR	Sinus rhythm	5,316	3,950,724	OTHER	SINUS	SR
STACH	Sinus tachycardia	2,838	1,192,025	OTHER	SINUS	STACH
AF	Atrial fibrillation	1,132	597,769	AF	AF+AFLT	AF
SBRAD	Sinus bradycardia	1,608	198,432	OTHER	SINUS	SBRAD
VPACE	Ventricular pacing	282	126,810	OTHER	OTHER	VPACE
AVPACE	Atrioventricular pacing	166	67,719	OTHER	OTHER	AVPACE
AFLT	Atrial flutter	210	44,811	AFLT	AF+AFLT	AFLT
APACE	Atrial pacing	145	44,415	OTHER	OTHER	APACE
SARRH	Sinus arrhythmia	105	7,224	OTHER	SINUS	SARRH
JR	Junctional rhythm	78	6,823	OTHER	OTHER	JR
SVTACH	Supraventricular tachycardia	193	6,342	OTHER	OTHER	SVTACH
MATACH	Multifocal atrial tachycardia	16	1,725	OTHER	OTHER	MATACH
VTACH	Ventricular tachycardia	53	1,273	OTHER	OTHER	VTACH
WAPACE	Wandering atrial pacemaker	7	854	OTHER	OTHER	OTHER
JTACH	Junctional tachycardia	16	571	OTHER	OTHER	OTHER
OTHER	Other	9	349	OTHER	OTHER	OTHER
PATACH	Paroxysmal atrial tachycardia	7	196	OTHER	OTHER	OTHER
VFIB	Ventricular fibrillation	9	147	OTHER	OTHER	OTHER
ASYS	Asystole	15	113	OTHER	OTHER	OTHER
IDIOV	Idioventricular rhythm	7	111	OTHER	OTHER	OTHER
1AVB	1 st degree AV block	304	111,729	exclude	exclude	exclude
LBBB	Left bundle branch block	45	22,667	exclude	exclude	exclude
RBBB	Right bundle branch block	43	13,092	exclude	exclude	exclude
2AVBM1	2 nd degree AV block Mobitz type 1	20	1,768	exclude	exclude	exclude
3AVB	3 rd degree AV block	27	1,360	exclude	exclude	exclude
2AVBM2	2 nd degree AV block Mobitz type 2	19	705	exclude	exclude	exclude
Total			6,399,754			

TABLE V: BP classification criteria ([31], [58]). Note that when systolic and diastolic blood pressure values fall into different categories, the hypertension stage is assigned according to the higher category, in accordance with established clinical guideline conventions [58].

BP Category	Systolic (SBP)	Operator	Diastolic (DBP)
Hypotension	< 90 mmHg	OR	< 60 mmHg
Normal	90–119 mmHg	AND	60–79 mmHg
Elevated	120–129 mmHg	AND	< 80 mmHg
Stage 1 Hypertension	130–139 mmHg	OR	80–89 mmHg
Stage 2 Hypertension	≥ 140 mmHg	OR	≥ 90 mmHg

TABLE VI: HR classification criteria for adults [32]. Note: sinus tachycardia is defined as a sinus node discharge rate > 100 times per minute, i.e., $HR > 100$ bpm.

HR Category	HR (bpm)
Bradycardia	< 60
Normal	60–100
Tachycardia	> 100

TABLE VII: BMI categories according to the WHO [33].

Category	BMI (kg/m^2)
Underweight	< 18.5
Normal	18.5–24.9
Overweight	25.0–29.9
Obese	≥ 30

TABLE VIII: Rhythm mapping between Liu et al. dataset [5] and *MIMIC-III-Ext-PPG* classification tasks

Liu et al. Rhythm	AF Task Mapping	SAA Task Mapping	ARRH Task Mapping
0: Sinus rhythm	OTHER	SINUS	SR
1: Premature ventricular contraction	Excluded	Excluded	Excluded
2: Premature atrial contraction	Excluded	Excluded	Excluded
3: Ventricular tachycardia	OTHER	OTHER	VTACH
4: Supraventricular tachycardia	OTHER	OTHER	SVTACH
5: AF	AF	AF+AFLT	AF

TABLE IX: Comparison of BP Estimation Performance

Study	Patients (n)	Data Duration (h)	SBP MAE (mmHg)	DBP MAE (mmHg)	Data Source/Subset
Ours	2,391	20,572	~ 16 – 17	~ 9 – 10	MIMIC-III (<i>MIMIC-III-Ext-PPG</i>)
Moulaeifard et al. [10]	1,474	2,357	~ 15 – 17	~ 9 – 10	MIMIC-III (PulseDB [59])
Sanches et al. (MIMIC-BP) [49]	1,524	380	\sim 13 – 14	~ 9 – 10	MIMIC-III (Custom Subset)

TABLE X: AUROC performance of heart rhythm detection across BP and HR categories (XResNet1d101). In-distribution baselines are from Table II. Dashes indicate insufficient samples. HTN: hypertension; HPN: hypotension.

Task	Rhythm	Baseline \uparrow	BP category \uparrow					HR category \uparrow		
			HPN	Normal	Elevated	Stage 1 HTN	Stage 2 HTN	Bradycardia	Normal	Tachycardia
AF	AF	0.96	0.95	0.99	0.99	0.99	0.97	0.88	0.96	0.97
	AFLT	0.77	0.80	0.77	0.78	0.80	0.84	0.74	0.76	0.86
SAA	SINUS	0.92	0.88	0.95	0.96	0.97	0.96	0.84	0.91	0.96
	AF+AFLT	0.95	0.96	0.99	0.99	0.99	0.97	0.87	0.95	0.97
ARRH	SR	0.93	0.92	0.95	0.96	0.96	0.94	0.72	0.86	0.76
	STACH	0.97	0.97	0.96	0.97	0.98	0.98	0.72	0.90	0.88
	AF	0.96	0.95	0.99	0.99	0.99	0.97	0.87	0.96	0.97
	SBRAD	0.96	0.97	0.96	0.97	0.98	0.97	0.75	0.90	0.58
	VPACE	0.79	0.73	0.80	0.91	0.82	0.65	0.82	0.77	0.72
	AVPACE	0.89	0.82	0.96	0.99	0.96	0.97	0.91	0.89	0.82
	AFLT	0.78	0.87	0.81	0.89	0.89	0.84	0.83	0.76	0.83
	APACE	0.80	0.73	0.79	0.78	0.87	0.76	0.61	0.80	0.96
	SARRH	0.61	0.89	0.78	0.86	0.90	0.85	0.93	0.80	0.73
	JR	0.62	0.47	0.42	0.81	–	0.62	0.86	0.53	0.63
	SVTACH	0.78	0.93	0.62	–	0.47	0.86	0.88	0.80	0.73
	MATACH	0.84	0.94	–	0.84	–	0.87	–	0.81	0.88
	VTACH	0.75	0.92	0.92	–	–	0.42	0.69	0.83	0.62

TABLE XI: Sensitivity (at specificity ≥ 0.8) and specificity (at sensitivity ≥ 0.8) across BP and HR categories (XResNet1d101). Values are reported as sensitivity/specificity. Baseline results are from Table II. Dashes indicate insufficient samples.

Task	Rhythm	Baseline \uparrow	BP category \uparrow					HR category \uparrow			
			HPN	Normal	Elevated	Stage 1 HTN	Stage 2 HTN	Bradycardia	Normal	Tachycardia	
AF	AF	0.92 / 0.98	0.92 / 0.98	0.99 / 0.99	0.99 / 0.99	0.99 / 0.99	0.99 / 0.99	0.94 / 0.99	0.79 / 0.78	0.93 / 0.99	0.96 / 0.97
	AFLT	0.62 / 0.61	0.70 / 0.73	0.61 / 0.65	0.54 / 0.70	0.63 / 0.72	0.78 / 0.79	0.78 / 0.79	0.51 / 0.50	0.62 / 0.59	0.73 / 0.76
SAA	SINUS	0.89 / 0.86	0.77 / 0.78	0.97 / 0.91	1.00 / 0.95	0.99 / 0.96	0.99 / 0.93	0.99 / 0.93	0.70 / 0.74	0.87 / 0.84	0.97 / 0.95
	AF+AFLT	0.93 / 0.98	0.92 / 0.98	0.99 / 0.99	0.99 / 1.00	0.99 / 1.00	0.95 / 0.99	0.95 / 0.99	0.80 / 0.80	0.92 / 0.98	0.96 / 0.98
ARRH	SR	0.93 / 0.89	0.93 / 0.88	0.95 / 0.94	0.97 / 0.95	0.96 / 0.95	0.96 / 0.95	0.94 / 0.92	0.51 / 0.49	0.75 / 0.76	0.58 / 0.58
	STACH	0.97 / 0.97	0.97 / 0.98	0.96 / 0.97	0.97 / 0.98	0.97 / 0.98	0.97 / 0.98	0.98 / 0.97	0.67 / 0.13	0.85 / 0.85	0.80 / 0.78
	AF	0.94 / 0.96	0.92 / 0.98	0.99 / 0.99	0.99 / 1.00	0.99 / 1.00	0.99 / 1.00	0.96 / 0.98	0.80 / 0.80	0.93 / 0.98	0.96 / 0.97
	SBRAD	0.95 / 0.98	0.94 / 0.99	0.94 / 0.99	0.95 / 0.99	0.98 / 0.99	0.98 / 0.99	0.96 / 0.99	0.52 / 0.55	0.87 / 0.88	0.27 / 0.29
	VPACE	0.62 / 0.60	0.47 / 0.51	0.61 / 0.65	0.86 / 0.85	0.61 / 0.65	0.61 / 0.65	0.29 / 0.44	0.69 / 0.70	0.59 / 0.56	0.47 / 0.53
	AVPACE	0.81 / 0.81	0.73 / 0.69	0.94 / 0.95	1.00 / 0.99	0.98 / 0.95	0.98 / 0.95	0.96 / 0.96	0.89 / 0.86	0.79 / 0.79	0.61 / 0.60
	AFLT	0.65 / 0.60	0.79 / 0.79	0.57 / 0.71	0.85 / 0.82	0.85 / 0.84	0.85 / 0.84	0.77 / 0.79	0.55 / 0.67	0.60 / 0.63	0.64 / 0.60
	APACE	0.63 / 0.61	0.45 / 0.54	0.68 / 0.53	0.66 / 0.53	0.78 / 0.76	0.78 / 0.76	0.45 / 0.60	0.22 / 0.44	0.66 / 0.63	0.97 / 0.96
	SARRH	0.40 / 0.26	0.78 / 0.79	0.57 / 0.61	0.70 / 0.78	0.80 / 0.82	0.80 / 0.82	0.68 / 0.75	0.92 / 0.90	0.57 / 0.60	0.38 / 0.59
	JR	0.45 / 0.20	0.14 / 0.12	0.19 / 0.13	0.64 / 0.78	–	–	0.25 / 0.47	0.74 / 0.77	0.35 / 0.11	0.33 / 0.33
	SVTACH	0.65 / 0.54	0.96 / 0.87	0.42 / 0.34	–	–	0.03 / 0.33	0.69 / 0.75	0.78 / 0.80	0.57 / 0.63	0.97 / 0.96
	MATACH	0.72 / 0.72	0.83 / 0.90	–	1.00 / 0.84	–	–	1.00 / 0.87	–	0.65 / 0.68	0.80 / 0.78
	VTACH	0.60 / 0.49	0.90 / 0.86	0.97 / 0.89	–	–	–	0.15 / 0.19	0.62 / 0.40	0.67 / 0.69	0.52 / 0.25

TABLE XII: Performance (AUROC) across gender, BMI, and ethnicity categories (XResNet1D101). Baseline results are taken from Table II. Dashes indicate insufficient samples. The "Underweight" BMI category was excluded due to the insufficient number of samples.

Task	Rhythm	Baseline \uparrow	Gender \uparrow		BMI \uparrow			Ethnicity \uparrow			
			Female	Male	Normal	Overweight	Obese	White	Black	Asian	Hispanic
AF	AF	0.96	0.95	0.96	0.92	0.92	0.98	0.95	0.96	0.98	0.95
	AFLT	0.77	0.84	0.75	0.72	0.75	0.75	0.74	0.93	–	–
SAA	SINUS	0.92	0.91	0.93	0.84	0.93	0.96	0.93	0.93	0.98	0.82
	AF + AFLT	0.95	0.95	0.95	0.93	0.93	0.97	0.95	0.95	0.98	0.95
ARRH	SR	0.93	0.93	0.92	0.87	0.92	0.95	0.93	0.95	0.98	0.91
	STACH	0.97	0.97	0.97	0.96	0.98	0.97	0.97	0.97	0.99	0.98
	AF	0.96	0.95	0.96	0.94	0.93	0.97	0.95	0.97	0.98	0.95
	SBRAD	0.96	0.96	0.96	0.98	0.96	0.95	0.97	0.97	0.89	0.91
	VPACE	0.79	0.71	0.84	0.65	0.88	0.95	0.86	–	0.97	0.95
	AVPACE	0.89	0.85	0.91	0.82	0.91	0.89	0.90	–	–	0.85
	AFLT	0.78	0.84	0.77	0.76	0.77	0.79	0.76	0.88	–	–
	APACE	0.80	0.87	0.73	0.86	0.71	0.82	0.80	–	–	0.63
	SARRH	0.61	0.56	0.78	0.80	0.91	0.53	0.50	0.88	–	0.84
	JR	0.62	0.75	0.59	0.18	0.42	0.82	0.45	0.96	–	–
	SVTACH	0.78	0.80	0.73	0.80	0.64	0.93	0.73	0.82	0.97	0.94
	MATACH	0.84	0.93	0.75	0.90	0.94	0.84	0.83	–	–	–
	VTACH	0.75	0.86	0.66	0.80	0.80	–	0.84	0.39	0.74	0.79

TABLE XIII: Sensitivity (at specificity ≥ 0.8) and specificity (at sensitivity ≥ 0.8) across demographic groups (XResNet1d101). Values are reported as sensitivity/specificity. Baseline results are from Table II. Dashes indicate insufficient samples.

Task	Rhythm	Baseline \uparrow	Gender \uparrow		BMI \uparrow			Ethnicity \uparrow			
			Female	Male	Normal	Overweight	Obese	White	Black	Asian	Hispanic
AF	AF	0.92 / 0.98	0.92 / 0.98	0.93 / 0.98	0.89 / 0.94	0.87 / 0.92	0.97 / 0.99	0.90 / 0.97	0.95 / 0.98	0.96 / 0.99	0.93
	AFLT	0.62 / 0.61	0.74 / 0.74	0.60 / 0.59	0.49 / 0.53	0.54 / 0.60	0.70 / 0.52	0.92 / 0.58	0.89 / 0.91	–	–
SAA	SINUS	0.89/0.86	0.86/0.84	0.91/0.88	0.69/0.72	0.92/0.88	0.97/0.94	0.93/0.89	0.93/0.91	0.99/0.98	0.66/0.62
	AF+AFLT	0.93/0.98	0.93/0.98	0.93/0.98	0.90/0.94	0.88/0.93	0.96/0.99	0.92/0.97	0.93/0.96	0.97/0.99	0.91/0.91
ARRH	SR	0.93/0.89	0.93/0.90	0.92/0.89	0.80/0.80	0.92/0.88	0.96/0.94	0.93/0.90	0.96/0.93	0.99/0.98	0.88/0.84
	STACH	0.97/0.97	0.96/0.97	0.97/0.98	0.95/0.95	0.97/0.98	0.97/0.89	0.96/0.97	0.97/0.98	0.99/0.99	0.98/0.98
	AF	0.94/0.96	0.93/0.97	0.94/0.97	0.91/0.94	0.88/0.92	0.97/0.98	0.93/0.97	0.97/0.97	0.96/0.99	0.93/0.93
	SBRAD	0.95/0.98	0.94/0.98	0.95/0.98	0.96/0.99	0.94/0.98	0.92/0.99	0.95/0.98	0.97/0.98	0.88/0.92	0.85/0.95
	VPACE	0.62/0.60	0.46/0.48	0.73/0.73	0.37/0.39	0.83/0.84	0.94/0.92	0.77/0.78	–	0.98/0.93	0.98/0.92
	AVPACE	0.81/0.81	0.73/0.73	0.86/0.88	0.67/0.69	0.87/0.89	0.85/0.88	0.85/0.86	–	–	0.69/0.71
	AFLT	0.65/0.60	0.76/0.75	0.63/0.62	0.60/0.63	0.59/0.62	0.70/0.69	0.61/0.61	0.84/0.84	–	–
	APACE	0.63/0.61	0.78/0.78	0.49/0.52	0.78/0.78	0.36/0.56	0.65/0.54	0.65/0.63	–	–	0.19/0.49
	SARRH	0.40/0.26	0.33/0.22	0.64/0.51	0.62/0.64	0.89/0.86	0.23/0.28	0.26/0.21	0.77/0.77	–	0.64/0.75
	JR	0.45/0.20	0.65/0.43	0.40/0.19	0.00/0.06	0.16/0.13	0.73/0.65	0.22/0.13	0.95/0.94	–	–
	SVTACH	0.65/0.54	0.71/0.67	0.53/0.43	0.65/0.67	0.45/0.29	0.97/0.89	0.57/0.46	0.69/0.64	1.00/0.96	0.93/0.95
	MATACH	0.72/0.72	0.94/0.90	0.49/0.60	0.93/0.87	0.91/0.87	0.72/0.75	0.70/0.71	–	–	–
VTACH	0.60/0.49	0.70/0.73	0.53/0.29	0.49/0.63	0.72/0.71	–	0.77/0.76	0.22/0.16	0.50/0.51	0.60/0.61	

TABLE XIV: Mapping of original MIMIC-III ethnicity labels to aggregated ethnicity groups, based on U.S. Office of Management and Budget Statistical Policy Directive No. 15 (1997) [34]. It is worth noting that due to extremely small numbers of subjects in certain categories (e.g., Caribbean Island, $n = 1$; American Indian/Alaska Native, $n = 2$; Native Hawaiian/Pacific Islander, $n = 2$; multiracial, $n = 17$), these groups were consolidated into the “OTHER” category to ensure statistical stability of subgroup analyses.

Original Ethnicity Label	Aggregated Group
WHITE	White
WHITE - RUSSIAN	White
WHITE - EASTERN EUROPEAN	White
WHITE - OTHER EUROPEAN	White
WHITE - BRAZILIAN	White
PORTUGUESE	White
MIDDLE EASTERN	White
BLACK/AFRICAN AMERICAN	Black
BLACK/AFRICAN	Black
BLACK/CAPE VERDEAN	Black
BLACK/HAITIAN	Black
ASIAN	Asian
ASIAN - CHINESE	Asian
ASIAN - ASIAN INDIAN	Asian
ASIAN - CAMBODIAN	Asian
ASIAN - VIETNAMESE	Asian
ASIAN - OTHER	Asian
ASIAN - FILIPINO	Asian
ASIAN - KOREAN	Asian
ASIAN - JAPANESE	Asian
HISPANIC OR LATINO	Hispanic
HISPANIC/LATINO - PUERTO RICAN	Hispanic
HISPANIC/LATINO - DOMINICAN	Hispanic
HISPANIC/LATINO - GUATEMALAN	Hispanic
HISPANIC/LATINO - CENTRAL AMERICAN (OTHER)	Hispanic
HISPANIC/LATINO - SALVADORAN	Hispanic
HISPANIC/LATINO - MEXICAN	Hispanic
HISPANIC/LATINO - COLOMBIAN	Hispanic
HISPANIC/LATINO - HONDURAN	Hispanic
HISPANIC/LATINO - CUBAN	Hispanic
OTHER	Other
UNKNOWN/NOT SPECIFIED	Other
UNABLE TO OBTAIN	Other
PATIENT DECLINED TO ANSWER	Other
AMERICAN INDIAN/ALASKA NATIVE	Other
NATIVE HAWAIIAN OR OTHER PACIFIC ISLANDER	Other
MULTI RACE ETHNICITY	Other
CARIBBEAN ISLAND	Other